Chalcogenide Letters Vol. 22, No. 2, February 2025, p. 131 - 142

Structural and optical properties of ZnS/rGO nanocomposites optoelectronic devices

A. M. Abdel-Daiem [a], M. Ahmed [a,*], E. R. Shaaban [b,*]
[a] *Department of Physics: Faculty of Science, King Abdulaziz University, 80203, Jeddah, Saudi Arabia*
[b] *Physics Department: Faculty of Science, Al-Azhar University, P.O. 71452, Assiut, Egypt*

This paper investigates the impact of reduced graphene oxide (rGO) addition on the structural and optical properties of ZnS nanocomposites. The study began with the synthesis of graphene oxide (GO) through the oxidation of natural graphite powder. This process involved using potassium permanganate in a mixture of sulfuric and phosphoric acids, maintained at 50°C for 48 hours. The reaction was terminated using hydrogen peroxide, followed by purification and drying, yielding 1.5 grams of GO. The preparation of ZnS/GO nanocomposites involved dissolving zinc acetate and varying quantities of GO in water, adjusting the pH, and incorporating sodium sulfide. This mixture underwent heating in an autoclave at 180°C for 12 hours, followed by washing and freezing, resulting in ZnS-RGO composites with differing GO contents. The resulting products were categorized as ZnS-0rGO, ZnS-5rGO, ZnS-10rGO, ZnS-15rGO, and ZnS-20rGO. To characterize these composite samples, the researchers employed several analytical techniques, including thermogravimetric analysis (TGA), X-ray diffraction (XRD) analysis, X-ray Photoelectron Spectroscopy (XPS), and UV-vis spectroscopy. This comprehensive approach allowed for a thorough examination of the effects of rGO incorporation on the nanocomposite's properties. The X-ray diffraction (XRD) results showed increased diffraction intensity with higher rGO content, attributed to improved crystallinity. The crystallite size and lattice strain also increased, with rGO providing nucleation sites. Optical analysis revealed that rGO increased absorbance and decreased the optical band gap, likely due to enhanced free charge carriers. The extinction coefficient and nonlinear refractive index both increased with rGO content, attributed to rGO's high polarizability and light-matter interactions.

(Received October 31, 2024; Accepted February 6, 2025)

Keywords: ZnS, ZnS-rGO composite, XRD, XPS, Optical parameters

1. Introduction

Zinc sulfide (ZnS) nanocomposites have emerged as versatile materials with a range of valuable properties that make them suitable for diverse applications. These nanocomposites are characterized by their exceptional transparency across the visible and infrared spectrum, exhibiting high optical transmittance that renders them ideal for use in various optical devices. A key feature of ZnS is its wide band gap, approximately 3.6 eV, which contributes significantly to its insulating properties. This characteristic expands its potential applications in the field of electronics. Furthermore, ZnS nanocomposites demonstrate impressive chemical stability and resistance to environmental degradation, ensuring their longevity and reliability in various operating conditions. Another notable attribute is the strong adhesion that ZnS films and nanocomposites typically show to substrates, making them excellent candidates for coating applications. The versatility of ZnS nanocomposites is further enhanced by the variety of fabrication methods available, including chemical vapor deposition, sputtering, and thermal evaporation. These diverse properties and flexible manufacturing techniques contribute to the widespread utility of ZnS nanocomposites across multiple fields, from optics and electronics to protective coatings and beyond [1-3]. Adding dopants or other materials to ZnS can significantly alter their properties. For instance, doping with elements

* Corresponding authors: mhafidh@kau.edu.sa
https://doi.org/10.15251/CL.2025.222.131

like Al, Cu, or Mn can enhance electrical conductivity, transforming ZnS from insulating to semiconductors.

The incorporation of dopants can significantly alter the optical characteristics of materials, including their band gap and refractive index. These changes are dependent on both the nature of the dopant and its concentration within the host material. As a result, the material's transparency and light absorption properties can be modulated, leading to shifts in its optical behavior. Such modifications in optical properties allow for the tailoring of materials for specific applications in optics and photonics. Mechanical properties, including hardness and adhesion to substrates, can also improve with the right additives. Furthermore, doping can affect the crystallinity and surface morphology, leading to smoother. These modifications can expand ZnS's applications in optoelectronics, sensors, and photovoltaic devices [4-7].

Reduced graphene oxide (rGO) has emerged as a crucial additive in materials science, owing to its remarkable combination of properties. This two-dimensional carbon material boasts exceptional electrical conductivity, superior thermal characteristics, and outstanding mechanical strength. The high surface area of rGO makes it particularly valuable for enhancing the performance of composite materials, especially in the realm of energy storage. When incorporated into batteries and supercapacitors, rGO can significantly boost their efficiency and capacity. Beyond energy applications, rGO's addition to various materials can lead to substantial improvements in mechanical properties, including increased strength, enhanced flexibility, and improved durability. The thermal conductivity of rGO is another notable feature, making it an excellent choice for applications requiring efficient heat dissipation, such as in electronic components. These multifaceted attributes of rGO underscore its versatility and importance as an additive across a wide range of technological and industrial applications. The oxygen functional groups present in rGO allow for improved dispersion in matrices, enhancing the overall homogeneity. Additionally, its tunable surface chemistry facilitates interactions with various materials, making rGO versatile for a range of applications, from sensors to catalysis [8-10].

Reduced graphene oxide (rGO) can significantly impact the properties of composite materials when used as an additive, it introduces multifunctionality, enabling composites to combine electrical, mechanical, and thermal properties for a wide range of applications in electronics, energy, and sensing technologies. Adding rGO enhances the electrical conductivity, transforming insulating or semiconducting materials into highly conductive layers, beneficial for applications like transparent conductive materials and sensors [11]. On the other side, rGO improves the mechanical durability and flexibility of nanomaterial making them more resistant to cracking, bending, or external stresses, especially in flexible electronics [12]. With its high thermal conductivity, rGO can help dissipate heat more efficiently, which is crucial for high-performance electronic and optoelectronic devices [13]. The addition of rGO can modify the optical transmittance of the medium, potentially reducing transparency while improving light absorption for applications like solar cells or photodetectors [14]. rGO can also improve the chemical resistance of composites, making them more stable in harsh environments, thereby increasing their lifespan [15]. Therefore, this study was performed to assess the impact of rGO on the structural and optical properties of ZnS nanocomposites for optical applications.

2. Experimental work

The synthesis of graphene oxide (GO) involved the oxidation of natural graphite powder through a carefully controlled process. The procedure began with combining 0.75 grams of graphite and 4.5 grams of potassium permanganate ($KMnO_4$). To this mixture, a solution comprising 90 ml of sulfuric acid (H2SO4) and 10 ml of phosphoric acid (H_3PO_4) was slowly introduced. The reaction was then maintained at a constant temperature of 50˚C for an extended period of 48 hours. This meticulous approach ensured the thorough oxidation of graphite, resulting in the formation of graphene oxide. The mixture's color shifted from dark green to light purple. After cooling and adding 0.75 ml of hydrogen peroxide (H_2O_2) to halt the reaction, the suspension turned dark yellow, indicating the formation of GO.

Following the oxidation process, the resulting suspension underwent centrifugation at 5000 rpm for 10 minutes. The material was then subjected to a washing procedure using hydrochloric acid and deionized water. To complete the GO preparation, the product was dried at 60˚C for 2 hours, resulting in approximately 1.5 grams of GO powder from the initial 0.75 grams of graphite. The synthesis of ZnS/rGO nanocomposites employed a hydrothermal method. This process began with dissolving 0.75 mmol of zinc acetate dihydrate $Zn(CH_3COO)_2.2H_2O$ and varying quantities of GO powder (0, 5, 10, 15, 20% relative to the ZnS amount) in 25 ml of deionized water. The solution's pH was adjusted to about 9 using ammonia water, accompanied by ultrasonic treatment. In a separate step, 0.75 mmol of sodium sulfide nonahydrate ($Na_2S·9H_2O$) was dissolved in 15 ml of deionized water, also with ultrasonic treatment. This Na2S solution was then introduced dropwise into the zinc acetate and GO mixture, which was continuously stirred magnetically for 30 minutes to ensure thorough mixing and reaction

The resulting mixture was subsequently transferred to a Teflon-lined autoclave and subjected to heating at 180°C for 12 hours. Following the reaction, the products underwent a thorough washing process using deionized water and ethanol, after which they were freeze-dried to obtain ZnS-rGO nanocomposites with varying GO contents. These samples were labeled according to their composition, ranging from pure ZnS to rGO-(5, 10, 15, 20%) ZnS, and coded as ZnS-0rGO, ZnS-5rGO, ZnS-10rGO, ZnS-15rGO, and ZnS-20rGO. To investigate the thermal properties of these ZnS-rGO nanocomposites, thermogravimetric analysis (TGA) was conducted using a Shimadzu 50 instrument. The TGA experiments were performed in static air, with a heating rate of 10°C per minute, covering a temperature range from room temperature to 800°C. For each analysis, approximately 6 mg of sample was placed in an alumina crucible without compression, and the thermogram was recorded using an open aluminum pan as the reference material. Additionally, crystallographic examination of the samples was carried out using an X-ray diffractometer (XRD, Cu-Kα = 1.54056 Å, Philips diffraction 1710), providing insights into the structural characteristics of the nanocomposites. The composite's elemental makeup was analyzed using energy-dispersive X-ray spectroscopy (EDXS). To measure UV-Vis absorption spectra, a Shimadzu UV-3600 plus UV-VIS-NIR Spectrophotometer was employed at ambient temperature, covering wavelengths from 300 to 750 nm.

3. Results and discussion

3.1. Thermogravimetric analysis (TGA)

Fig. 1 shows the TGA (thermogravimetric analysis) curves of the samples provide insight into the extent of reduction of graphene oxide (GO). The data indicates that pristine GO experiences significant weight loss, approaching 100 wt.%, when heated to 615 °C. This weight loss can be attributed to three main processes: The first is as the temperature rises from room temperature to nearly 100 °C, small water molecules that are chemically adsorbed on the surface of GO begin to evaporate. This initial weight loss reflects the removal of these moisture components. The second**,** at the temperature between 100 and 300 °C, there is a substantial reduction in the material's weight due to the decomposition and release of various oxygen-containing functional groups present in the GO structure. This process is critical as it indicates a transition towards a more reduced form of graphene. The third at the temperature between 300 to 610 °C, the carbon-chain framework of GO starts to degrade, contributing to further weight loss. This phase represents the breakdown of the carbon structure, leading to the loss of mass. In contrast, the ZnS sample exhibits minimal mass loss. This is primarily due to the oxidation of ZnS into ZnO, which does not result in significant weight reduction under the same thermal conditions. For the ZnS-5% rGO to the ZnS-20% rGO samples, there is a notable a weight loss of decrease with increasing rGo content between 100 and 300 °C. This decrease is attributed to the degradation of any remaining oxygen-containing functional groups, indicating that the GO has been sufficiently reduced to reduced graphene oxide (RGO). This suggests that the reduction process was effective, as most of the oxygen functionalities have been removed.

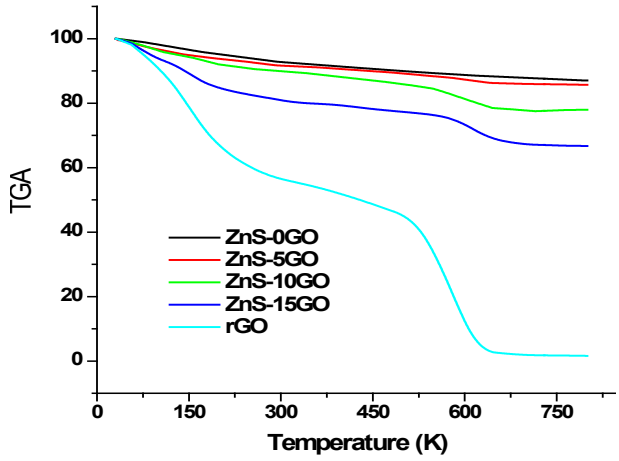

Fig. 1. Thermogravimetric analysis (TGA) of varies composites.

3.2. X-ray diffraction analysis

Figure 2 presents the X-ray diffraction (XRD) patterns for graphene oxide (GO) and reduced graphene oxide (rGO) samples, both derived from natural graphite. For the GO samples, the XRD pattern prominently features a diffraction peak at $2\theta = 10.84°$, which corresponds to the (002) plane. This peak indicates an average d-spacing of approximately 0.88 nm, characteristic of the interlayer distance in GO. Following the hydrothermal reduction process, the XRD pattern of the rGO samples shows a significant change. The original peak at $2\theta = 10.84°$ associated with GO has disappeared. Instead, a new broad peak appears at $2\theta = 26.18°$, corresponding to the (002) plane of rGO, with an average d-spacing of around 0.34 nm. This shift to a broader and more intense peak reflects the reduction of GO to rGO, which is characterized by a decrease in the interlayer spacing due to the removal of oxygen-containing functional groups.

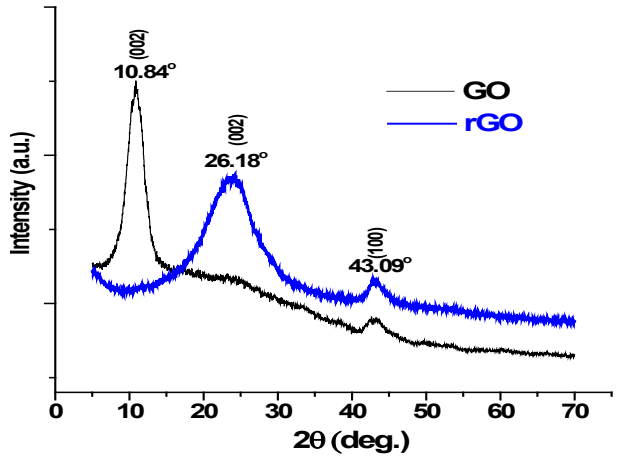

Fig. 2. XRD patterns of the pristine GO and RGO.

The X-ray diffraction (XRD) patterns of ZnS/rGO nanocomposites with different rGO weight ratios are shown in Figure 3 (a). These patterns exhibit a strong similarity to those of pure ZnS. Figure 3 (b) illustrates the peak deconvolution, revealing five distinct peaks at 26.98°, 28.55°, 30.60°, 47.65°, and 56.49°. These peaks correspond to the (100), (002), (101), (110), and (112) crystal planes, respectively, which are characteristic of the wurtzite-phase ZnS structure (JCPDS No. 36–1450). Notably, the patterns for ZnS-rGO samples do not display any distinct peaks for rGO, likely due to its low content in the composites. This suggests that the addition of rGO does not hinder the growth of ZnS crystal orientations; instead, rGO acts as a supportive framework for ZnS

development. The XRD patterns reveal that while ZnS and ZnS/rGO nanocomposites exhibit similar peaks, their intensities differ. Specifically, the intensity decreases with increasing rGO content. This reduction in XRD intensity can be explained by the dilution effect, where a higher rGO proportion means less ZnS is present to contribute to the diffraction signal. Additionally, interactions between ZnS and rGO could influence the crystallinity of ZnS. For example, rGO may impede the growth of ZnS crystals or induce lattice strain, further contributing to the overall decrease in XRD peak intensity [16-18].

Based on the Debye-Scherer model, Eqs. 1 and 2 were used to determine the crystallite average size (D) as well as the lattice strain (e) of the tested samples based on XRD.

$$D = \frac{0.94\lambda}{\beta\, cos\theta} \tag{1}$$

$$e = \frac{\beta}{4tan\theta} \tag{2}$$

These equations establish a relationship between the crystallite size (D) and lattice strain (e) with key X-ray diffraction parameters: the primary X-ray wavelength (λ), the angle of diffraction (θ), and the full width at half maximum (FWHM) of the diffraction peak, denoted as β [19].

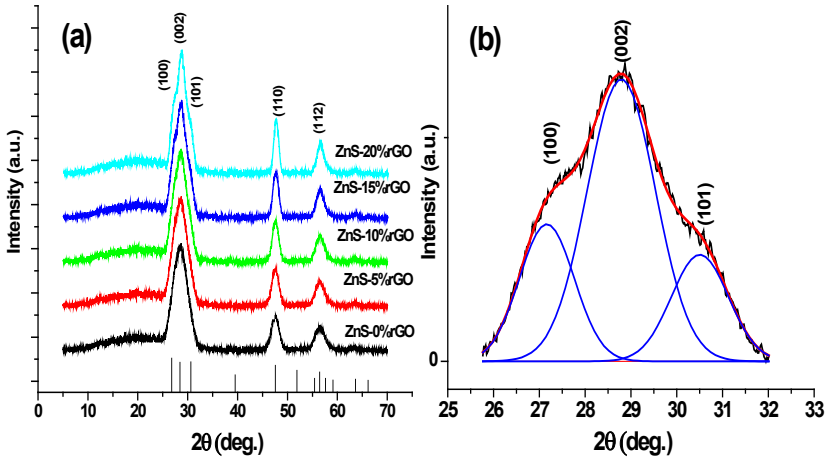

Fig. 2. XRD patterns of ZnS/rGO nanocomposites.

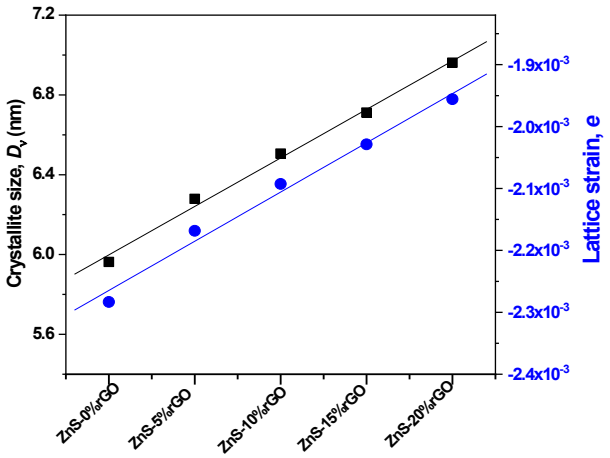

Fig. 4. Lattice strain and crystal size versus rGO content.

As shown in Figure 4, the calculations resulted in an increase in the value of the crystal size (*D*) as well as an increase in the value of the lattice strain (e) as rGO was added to ZnS nanocomposites. This observed increment in the crystal size (D) can be attributed to the fact that rGO provides additional nucleation sites in the composite. As the content of rGO increases, these sites facilitate the crystallization of materials around the rGO sheets, resulting in the growth of larger crystallites [20-21]. Meanwhile, the observed increase in lattice strain indicates a deviation from the perfect crystal structure. This deviation can be attributed to various factors, including the presence of impurities or defects within the crystal structure. In other words, rGO has a different lattice structure and atomic arrangement compared to many host materials (e.g., polymers, ceramics, or metals) with which it is combined. As rGO content increases, the structural mismatch between rGO and the host material can induce strain at the interface [22-23].

3.3. Energy dispersive X-Ray spectroscopy analysis of ZnS/rGO nanocomposites

Figure 5 (a, b) represents the EDAX of ZnS-5% rGO and ZnS-20% rGO nanocomposites provides valuable information about their elemental composition. The EDX spectra typically reveal the presence of key elements such as zinc (Zn), sulfur (S), and carbon (C), which are essential components of the ZnS/rGO nanocomposite. The presence of ZnS in the composite would be confirmed by the appearance of characteristic peaks corresponding to zinc and sulfur. The intensity of these peaks might fluctuate depending on the amount of rGO incorporated. Carbon peaks, attributable to the reduced graphene oxide, would also be present. The intensity of these carbon peaks would offer insights into the rGO content within the composite Depending on the synthesis process, trace amounts of other elements, such as oxygen (O) or impurities, may also be detected. These could arise from residual functional groups in rGO or from the synthesis environment.

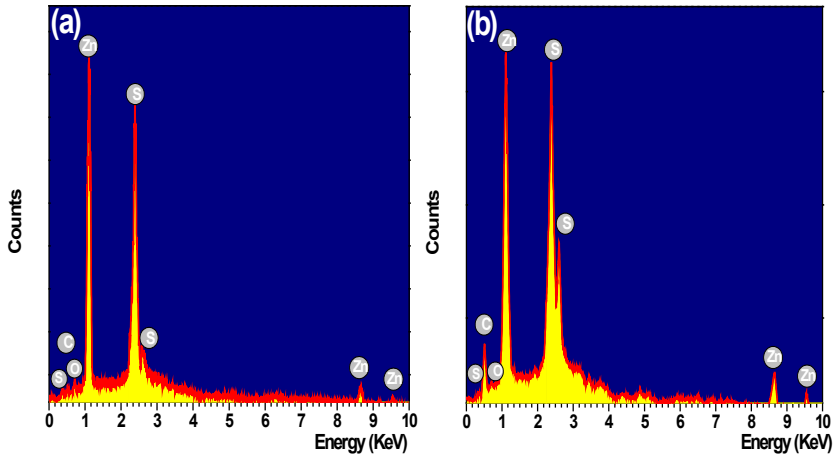

Fig. 5. The energy dispersive X-ray spectroscopy analysis (EDAX) of (a) ZnS-5% rGO and (b) ZnS-20% rGO nanocomposites.

3.4. Optical characterization

The optical characteristics of reduced graphene oxide (rGO)-doped materials are critical to their performance in numerous applications. rGO doping can drastically modify the electrical structure and optical behavior, resulting in improved absorption and emission properties. This alteration increases the efficiency of materials used in optoelectronic devices like sensors, photo-detectors, and solar cells. Furthermore, the tunable optical features of rGO-doped materials make them suitable for advanced technologies such as flexible electronics and smart coatings. Understanding and maximizing these qualities can result in advances in material design and usefulness [24-25].

Figure 6 depicts the influence of rGO content on the optical absorbance of ZnS nanocomposites. It is obvious that given a fixed amount of rGo, absorbance values declined at two separate rates as the photon wavelength grew. The conversion point between these rates moved to

higher wavelengths as the rGo content rose. For a fixed wavelength, the absorbance value increased as the rGO concentration increased. These findings indicate that rGo altered the electronic structure of the ZnS by increasing the effective number of absorbers (free charge carriers) and/or decreasing the optical band gap value.

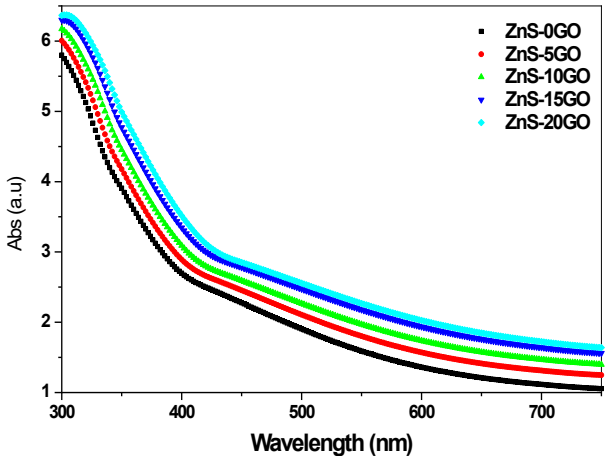

Fig. 6. The optical absorbance spectra of ZnS/rGO nanocomposites.

Because XPS is a powerful technique for studying changes in the electronic structure of materials, it was employed to confirm the veracity of the previous expectation. As shown in Figure 7, peak positions have not shifted, but peak shapes and intensities have changed. Changes in peak form or intensity can be attributed to changes in electrical structure or the existence of various chemical states [26-27].

The alteration in electronic structure suggests a corresponding change in the optical band gap, which can either decrease or increase. To compare the optical band gap values of the tested samples, the measured optical absorbance was utilized. Figure 8 depicts the plot of dA/dE against photon energies. This figure exhibits a single maximum limit in the dA/dE versus E curve, which corresponds to one optical energy gap.

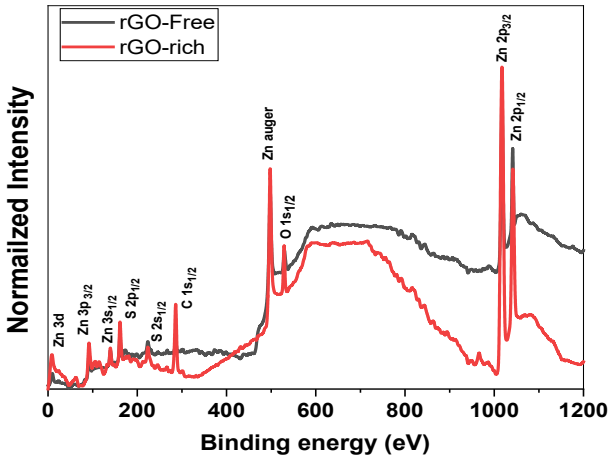

Fig. 7. XPS spectra of rGo-Free and ZnS-20%rGO sample.

Table 1 demonstrates the variation of the energy band gap (Eg) of ZnS with increasing rGO content. As the amount of rGO increases, the optical band gap (Eg) of ZnS decreases. This

observation indicates that rGO is incorporated into the ZnS lattice without segregation, meaning it integrates effectively into the ZnS structure without forming distinct phases. Generally, the reduction in the energy band gap can be linked to an increase in defect levels and/or strain. According to Davis and Mott, structural defects can generate localized states within the band gap. Consequently, as defect concentrations rise, the width of these localized states expands, leading to a smaller energy gap (Eg) for ZnS composites.

Table 1. The optical energy gap E_g, linear refractive index n, nonlinear refractive index n_2.

rGO	0	5	10	15	20
E_g eV	**3.82**	**3.75**	**3.71**	**3.67**	**3.63**
n	**2.05**	**2.06**	**2.07**	**2.08**	**2.09**
n_2 (esu)	**1.14081E-11**	**1.22E-11**	**1.27E-11**	**1.32E-11**	**1.37E-11**

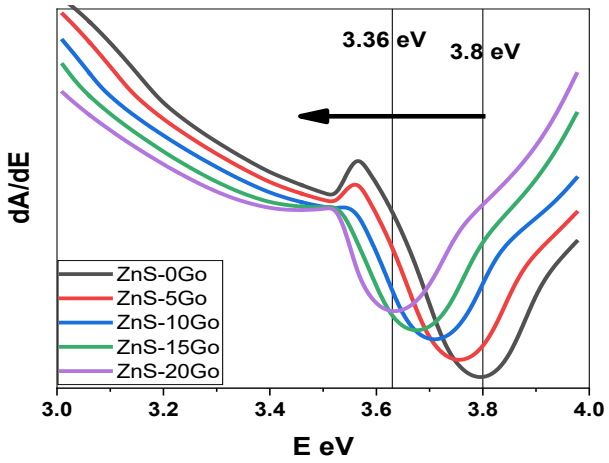

Fig. 8. dA/dE versus rGO content for all samples.

The extinction coefficient is important in optical characterization because it indicates how much light is absorbed as it travels through a material. It helps to determine the material's transparency and absorption effectiveness. This coefficient is critical for understanding a material's optical losses, particularly in applications such as solar cells, lenses, and optical coatings. Accurate measurements of the extinction coefficient are required when constructing devices with specific light transmission or reflection qualities. It also helps to understand the electrical structure and energy band gaps of materials [31-32].

The extinction coefficient (K) of ZnS-rGO nanocomposites was determined using Eq. 3, where t is the sample thickness (about 1 cm of the spectrophotometric cell). The spectral behavior of the extinction coefficient for these materials is depicted in Figure 9.

$$K = \frac{\alpha\lambda}{4\pi} \quad [33] \tag{3}$$

$$\alpha = 2.303\,\frac{A}{t} \quad [34] \tag{4}$$

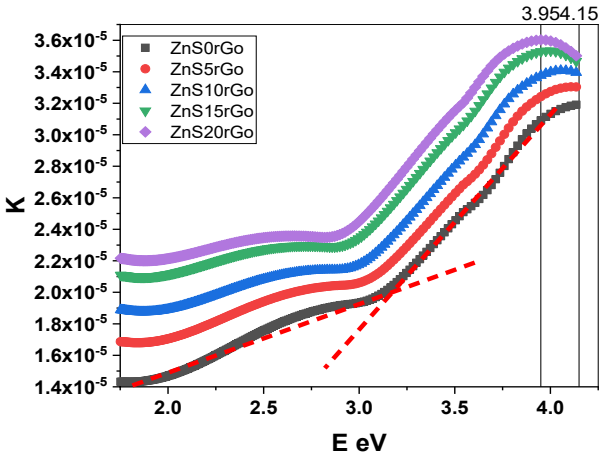

Fig. 9. Extinction coefficient versus rGO content for all samples.

Figure 9 shows that, as photon energy increased the extinction coefficient K increased with two different rates. Furthermore, the figure illustrates that the overall extinction coefficient increases with higher levels of rGo incorporation. This trend supports the significant influence of rGO doping on the optical properties of the composites, underscoring its potential relevance in various optoelectronic applications. Generally, the observed shift in dispersion energy may indicate that the presence of rGO enhances light attenuation through increased optical absorption [35].

The extinction coefficient (K) is associated with the nonlinear refractive index (n_2). Both involve the interaction of light with material, specifically how the material absorbs and refracts light at high intensities. Although linear absorption and intensity-dependent refractive behavior are distinct phenomena, high absorption (large K) can be associated with strong nonlinear optical characteristics in certain materials.

For example, materials with strong absorption resonances may display considerable nonlinear refractive effects as a result of the interaction between the material's electronic states and the incident light. Both properties are frequently dependent on the material's electrical structure and optical sensitivity at various wavelengths [36-37].

Accordingly, the nonlinear Refractive Index (n_2), which defines how a material's refractive index changes with the intensity of incident light, was calculated based on the optical band gap values according to the following set of equations.

$$n_2 = \varepsilon_o\,(n-1)^{5.27} \qquad [38] \qquad [5]$$

$$n = \sqrt{\frac{(3.44)^2}{E_g^{1/2}} - (3.44)^{1/2}} \qquad [39] \qquad [6]$$

The increase in both the linear and nonlinear refractive indices, see Table 1, with an increase in reduced graphene oxide (rGO) content can be explained as follows;

The rGO has a unique electronic structure, with delocalized π-electrons that contribute to strong light-matter interactions. As the rGO content increases, the density of these free carriers rises, enhancing the material's overall polarizability. This leads to an increase in both the linear and nonlinear refractive indices.

Also, rGO exhibits high optical polarizability due to its sp^2 hybridized carbon atoms, which enables stronger interactions with the electromagnetic field. As the rGO concentration increases, the material becomes more responsive to light, thereby increasing the linear refractive index [40-41].

Conversely, the nonlinear refractive index (n_2) is influenced by both the light's intensity and the material's third-order nonlinear susceptibility (χ^3). Reduced graphene oxide (rGO) demonstrates robust nonlinear optical characteristics, attributed to its substantial χ^3 value. As the concentration of

rGO increases, its impact on the nonlinear refractive index becomes more pronounced, resulting from intensified light-matter interactions and a greater density of excited charge carriers [40-43].

4. Conclusions

The research findings indicate that the addition of reduced graphene oxide (rGO) to zinc sulfide (ZnS) composites substantially alters their structural characteristics and optical behavior. X-ray diffraction analysis confirmed that rGO enhances the crystallinity of ZnS, increasing both the crystallite size and lattice strain. Optical measurements indicated that rGO doping improves absorbance and reduces the optical band gap, likely due to the presence of additional free charge carriers.

The extinction coefficient and nonlinear refractive index also increased with higher rGO content, reflecting rGO's strong light-matter interactions and high polarizability. These findings underscore the potential of rGO-doped ZnS in advanced optoelectronic applications, highlighting the benefits of rGO in optimizing material performance for various technological uses. Based on the findings of this study, rGO-doped ZnS could be applied in several advanced technologies, like rGO-doped ZnS composites could be applied in several advanced technologies like optoelectronic devices, transparent conductive materials, flexible electronics, sensors, photovoltaic devices, and smart coatings.

Acknowledgments

This project was funded by the Deanship of Scientific Research (DSR) at King Abdulaziz University, Jeddah, under grant no. (GPIP: 750-130-2024). The authors, therefore, acknowledge with thanks DSR for technical and financial support.

References

[1] Shakoury, R., Arman, A., Ţălu, Ş. et al., J Mater Sci: Mater Electron 31, 5262-5273 (2020); https://doi.org/10.1007/s10854-020-03086-3

[2] Grayeli, A., Sadeghi, M., Shakoury, R. et al., Opt Quant Electron 56, 1142 (2024); https://doi.org/10.1007/s11082-024-07039-6

[3] Hwang, D.H., Ahn, J.H., Hui, K.N. et al., Nanoscale Res Lett 7, 26 (2012); https://doi.org/10.1186/1556-276X-7-26

[4] Bipanko Kumar Mondal, Ahnaf Tahmid Abir, Jaker Hossain, Energy Technology; https://doi.org/10.1002/ente.202301329

[5] B. Das, I. Aguilera, U. Rau, T. Kirchartz, Adv. Optical Mater. 2022, 10, 2101947; https://doi.org/10.1002/adom.202101947

[6] Abdelhak Jrad, Manel Naouai, Amal Abdallah, Souad Ammar, Najoua Turki-Kamoun, Physica B: Condensed Matter, 603,2021,412776; https://doi.org/10.1016/j.physb.2020.412776

[7] Abdelhak Jrad, Manel Naouai, Souad Ammar, Najoua Turki-Kamoun, Materials Science in Semiconductor Processing, 130,2021,105825; https://doi.org/10.1016/j.mssp.2021.105825

[8] Feng, J., Ye, Y., Xiao, M. et al., Chem. Pap. 74, 3767-3783 (2020); https://doi.org/10.1007/s11696-020-01196-0

[9] Lesiak, B., Trykowski, G., Tóth, J. et al., J Mater Sci 56, 3738-3754 (2021); https://doi.org/10.1007/s10853-020-05461-1

[10] Abdolhosseinzadeh, S., Asgharzadeh, H., Seop Kim, H., Sci Rep 5, 10160 (2015); https://doi.org/10.1038/srep10160

[11] Anusuya, T., Prema, D. & Kumar, V., J Mater Sci: Mater Electron 33, 8935-8945 (2022); https://doi.org/10.1007/s10854-021-06979-z

[12] Yang, Y., Shen, H., Yang, J. et al., J. Electron. Mater. 50, 6991-6999 (2021); https://doi.org/10.1007/s11664-021-09201-2

[13] Lv, M., Wei, Q., Cao, S. et al., J Mater Sci: Mater Electron 32, 11727-11736 (2021); https://doi.org/10.1007/s10854-021-05797-7

[14] Aboraia, A.M., Yahia, I.S., Saad, M. et al., J Opt (2024); https://doi.org/10.1007/s12596-024-02092-6

[15] Allagui, A., Abdelkareem, M., Alawadhi, H., et al., Sci Rep 6, 21282 (2016); https://doi.org/10.1038/srep21282

[16] Kim, H., Abdala, A. A., Macosko, C. W. (2010), Macromolecules, 43(16), 6515-6530; https://doi.org/10.1021/ma100572e

[17] Dreyer, D. R., Park, S., Bielawski, C. W., Ruoff, R. S. (2010), Chemical Society Reviews, 39(1), 228-240; https://doi.org/10.1039/B917103G

[18] Pei, S., Cheng, H. M. (2012), Carbon, 50(9), 3210-3228; https://doi.org/10.1016/j.carbon.2011.11.010

[19] Holzwarth, U., Gibson, N., Nature Nanotech 6, 534 (2011); https://doi.org/10.1038/nnano.2011.145

[20] Stankovich, S., Dikin, D. A., Dommett, G. H. B., Kohlhaas, K. M., Zimney, E. J., Stach, E. A., Piner, R. D., Nguyen, S. T., Ruoff, R. S. (2006), Nature, 442(7100), 282-286; https://doi.org/10.1038/nature04969

[21] Eda, G., Chhowalla, M. (2010), Advanced Materials, 22(22), 2392-2415; https://doi.org/10.1002/adma.200903689

[22] Zhang, L., Sun, Y., Wang, Y., Zhao, H. (2012), Journal of Materials Science, 47(1), 343-350

[23] Wang, X., Zhi, L., Mullen, K. (2008), Nano Letters, 8(1), 323-327; https://doi.org/10.1021/nl072838r

[24] Zhang, H., Zhang, L. (2021), Advanced Functional Materials, 31(24), 2101037.

[25] Chen, L., Liu, W., Liu, Y. (2020), Journal of Materials Science, 55(14), 6035-6047.

[26] Wagner, C. D., Zibell, J. M., Moulder, J. F. (2017), Practical surface analysis: Auger and X-ray photoelectron spectroscopy (3rd ed.), John Wiley & Sons.

[27] Briggs, D., Seah, M. P. (1990), Practical surface analysis: Auger and X-ray photoelectron spectroscopy, John Wiley & Sons.

[28] Jimenez, J., Tomm, J.W. (2016), Optical Sciences, vol 202. Springer, Cham; https://doi.org/10.1007/978-3-319-42349-4_2

[29] Handbook of Ellipsometry, Vol., ed. by H.G. Tompkins, E.A. Irene (William Andrew, Inc. and Springer-Verlag GmbH & Co. KG, 2005)

[30] Ajay Kumar, Rajeev Kumar, Nancy Verma, A.V. Anupama, Harish K. Choudhary, Reji Philip, Balaram Sahoo, Optical Materials,108, 2020,110163; https://doi.org/10.1016/j.optmat.2020.110163

[31] Fox, M. (2010), Optical properties of solids (2nd ed.), Oxford University Press.

[32] Bohren, C. F., Huffman, D. R. (2008), Absorption and scattering of light by small particles, Wiley.

[33] Yariv, Amnon,Pochi Yeh. Photonics: Optical Electronics in Modern Communications. Oxford University Press, 2007,

[34] H.M. Gomaa, H.A. Saudi, H.Y. Zahran, et al., J. Opt Quant Electron 56 (2024) 211; https://doi.org/10.1007/s11082-023-05819-0

[35] Bonavolontà, C., Vettoliere, A., Falco, G. et al., Sci Rep 11, 13015 (2021); https://doi.org/10.1038/s41598-021-92518-z

[36] Boyd, R. W. (2020), Nonlinear optics (4th ed.), Academic Press.

[37] Shen, Y. R. (2003), The principles of nonlinear optics, Wiley-Interscience.

[38] Gomaa, H.M., Yahia, I.S., J Comput Electron 21, 1174-1179 (2022); https://doi.org/10.1007/s10825-022-01915-8

[39] Hosam M. Gomaa, I.S. Yahia, H.Y. Zahran, Physica B: Condensed Matter, 620,2021,413246; https://doi.org/10.1016/j.physb.2021.413246

[40] Bonaccorso, F., Sun, Z., Hasan, T., Ferrari, A. C. (2010), Nature Photonics, 4(9), 611-622; https://doi.org/10.1038/nphoton.2010.186

[41] Verma, S., Kar, K. K., Palkar, V. R. (2017), Journal of Materials Science, 52(6), 3174-3193.

[42] Zhang, H., Virally, S., Bao, Q., Ping, L. K., Massar, S., Godbout, N., Kockaert, P. (2012), Optics Letters, 37(11), 1856-1858; https://doi.org/10.1364/OL.37.001856

[43] Singh, V., Joung, D., Zhai, L., Das, S., Khondaker, S. I., Seal, S. (2011). Progress in Materials Science, 56(8), 1178-1271; https://doi.org/10.1016/j.pmatsci.2011.03.003